





Cite this: *Polym. Chem.*, 2018, **9**, 1593

# Oxidation-responsive micelles by a one-pot polymerization-induced self-assembly approach†

Fabian H. Sobotta,<sup>a,b</sup> Franziska Hausig,<sup>a,b</sup> Dominic O. Harz,<sup>a</sup> Stephanie Hoepfner,<sup>a,b</sup> Ulrich S. Schubert <sup>a,b</sup> and Johannes C. Brendel <sup>\*,a,b</sup>

The increased levels of reactive oxygen species (ROS) such as hydrogen peroxide in inflamed or cancerous tissue represent a promising trigger for the local and selective release of drugs at the affected areas. Despite new developments in the field of oxidation-responsive drug carrier systems, the preparation of the required materials remains in most cases tedious. Here, we present a novel system, which combines the advantages of a one-pot sequential controlled radical polymerization with the direct polymerization-induced self-assembly (PISA) process. By utilizing highly reactive acrylamide monomers, full conversion can be reached while maintaining a high chain end fidelity in RAFT polymerization, which enables the precise preparation of block copolymers or micelles, respectively, without intermediate purification steps. We demonstrate that the cyclic thioether *N*-acryloyl thiomorpholine is a versatile monomer for PISA resulting in a hydrophobic block, which upon oxidation can be transformed into a highly water-soluble sulfoxide. The micellar structures are tunable in size by the variation of the block length and feature a good sensitivity towards hydrogen peroxide even at low concentrations of 10 mM resulting in their disintegration. *In vitro* studies prove the uptake of these micelles into cells without signs of toxicity up to 500  $\mu\text{g mL}^{-1}$ . The straightforward preparation, the excellent biocompatibility and the selective disintegration in the presence of biologically relevant levels of hydrogen peroxide are features that certainly make the presented system an attractive new material for oxidation-responsive drug carriers.

Received 5th November 2017,  
Accepted 22nd December 2017

DOI: 10.1039/c7py01859b

rsc.li/polymers

## Introduction

ROS and reactive nitrogen species (RNS) play important roles as signaling molecules in various physiological processes.<sup>1–4</sup> However, when the oxidative stress levels exceed usual values, the increased stress results in the disruption of cellular homeostasis and causes severe damage to healthy tissue. Such increased levels of stress or ROS are mostly related to diseases including inflammatory disorders, diabetes or cancer.<sup>5–7</sup> Current therapeutic strategies to compensate these effects are mostly based on the administration of anti-inflammatory drugs, which are accompanied by several undesirable side effects arising from poor systemic selectivity and stability.<sup>8–10</sup> In this context, the development of nanocarriers, which are able to circulate freely through the blood, while releasing anti-inflammatory drugs only at the inflammation site and pro-

portional to its severity, is highly desirable. It also seems reasonable to exploit the high concentrations of ROS at inflammation sites ( $\sim 10\text{--}1000 \times 10^{-6} \text{ M}$ ) compared to that of healthy tissue ( $\sim 1\text{--}8 \times 10^{-6} \text{ M}$ ) as triggers for responsive and selective drug carrier systems.<sup>11</sup> Despite these still rather low concentrations, it has to be kept in mind that ROS comprises, besides the rather stable hydrogen peroxide, mostly a variety of very reactive species such as superoxide anion radicals, hydroxyl radicals, and other peroxides.<sup>12</sup> Therefore, higher concentrations of  $\text{H}_2\text{O}_2$  are commonly applied to compensate for these differences in reactivity.<sup>13–15</sup> Still, in comparison with the vast number of pH-, light- and temperature-responsive materials, to date, there is only a relatively small number of reported systems making use of oxidation as stimuli.<sup>14–17</sup> Polymer-based micelles equipped with redox-responsive groups have attracted the most attention, since they are not only able to embed many drugs but also release them selectively at the inflammatory location. In addition to the function as a drug carrier, the carrier itself may serve as an antioxidant by buffering the oxidative stress level at the inflammation site.

Besides selenides<sup>18–20</sup> or boronic esters<sup>21–23</sup> thioethers appear to be promising materials for oxidation-sensitive carriers. The oxidation of hydrophobic thioethers results in the formation of hydrophilic sulfoxides and/or sulfones, which

<sup>a</sup>Laboratory of Organic and Macromolecular Chemistry (IOMC), Friedrich Schiller University Jena, Humboldtstrasse 10, 07743 Jena, Germany. E-mail: johannes.brendel@uni-jena.de

<sup>b</sup>Jena Center for Soft Matter (JCSM), Friedrich Schiller University Jena, Philosophenweg 7, 07743 Jena, Germany

†Electronic supplementary information (ESI) available. See DOI: 10.1039/c7py01859b

can induce a morphological transition, such as the swelling or the degradation of aggregates, and, as a consequence, release an encapsulated bioactive compound. However, reports on well-defined polymers, which are able to form micelles and comprise oxidation-responsive thioethers, remain scarce and are mostly limited to poly(propylene sulfides) or polyethers.<sup>13,24–26</sup>

Here, we report the controlled one-pot synthesis and polymerization-induced self-assembly (PISA) of a novel thioether-based block copolymer using the versatile reversible addition–fragmentation chain transfer (RAFT) process. Several pioneering studies have already demonstrated that PISA represents a powerful technique to generate nanostructures in a variety of morphologies.<sup>27–32</sup> The PISA process overcomes the drawbacks of conventional methods for micelle preparation, including low nanoparticle concentration and time-consuming purification steps,<sup>33–35</sup> and even enables a simultaneous self-assembly and guest molecule encapsulation.<sup>36</sup> Moreover, a high control over morphology can be reached by adjusting the packing parameter of the hydrophobic block during the PISA process.<sup>37,38</sup> In our attempt, we combine these advantages with the high reactivity of acrylamides, such as *N*-acryloylmorpholine (NAM), which can reach quantitative conversions with high chain-end retention in the RAFT process.<sup>39–42</sup> PNAM is already known to show high biocompatibility, low protein adsorption and low toxicity.<sup>43,44</sup> For the hydrophobic block in the PISA process, we envisaged a structurally similar monomer based on thiomorpholine, which provides the desired oxidation-responsive thioether moiety. This novel *N*-acryloylthiomorpholine (NAT) does not only enable a PISA process but also reaches full conversions similar to NAM with low initiator concentrations. Therefore, several block copolymers consisting of PNAM as hydrophilic and PNAT as hydrophobic blocks were synthesized in aqueous solutions resulting in well-defined micelles of various sizes. These nanostructures were examined for their biocompatibility and their oxidation-responsiveness using H<sub>2</sub>O<sub>2</sub>. The structural changes were monitored by spectroscopy studies using Nile red and dynamic light scattering (DLS) measurements.

## Experimental part

### Materials and methods

All chemical and solvents were purchased from Sigma-Aldrich, Merck and TCI Chemicals and, if not mentioned otherwise, used without further purification. NAT was synthesized according to a previously reported procedure.<sup>45</sup> 2-(Butylthiocarbonylthio)propanoic acid was prepared as previously reported.<sup>46</sup> P(NAM<sub>50</sub>-*b*-NAT<sub>30</sub>) was prepared by stirring **P3** overnight in 0.1 M H<sub>2</sub>O<sub>2</sub> and subsequent lyophilization.

<sup>1</sup>H-NMR was performed at room temperature on a Bruker AC 300 MHz spectrometer in CDCl<sub>3</sub> or DMSO-*d*<sub>6</sub>. Size-exclusion chromatography (SEC) of the polymers was performed on a Shimadzu system equipped with an SCL-10A system controller, an LC-10AD pump, a RID-10A refractive index detector and

a PSS SDV column with *N,N*-dimethylacetamide (DMAc) + 0.21% LiCl. The column oven was set to 50 °C. DLS was performed on a ZetaSizer Nano ZS (Malvern, Herrenberg, Germany) equipped with a He–Ne laser operating at a wavelength of  $\lambda = 633$  nm. Counts were detected at an angle of 173°. The particle size was approximated as the effective diameter (*Z*-average) obtained by the cumulants method assuming a spherical shape. All measurements were conducted at 25 °C in semi-micro cuvettes after an equilibration of 60 s in triplicate. Every measurement included 10 runs, in which every run took 10 seconds. Apparent hydrodynamic radii were calculated using the Stokes–Einstein eqn (1):

$$R_h = \frac{kT}{6\pi\eta D} \quad (1)$$

$R_h$  = hydrodynamic radius,  $k$  = Boltzmann constant,  $T$  = absolute temperature,  $\eta$  = viscosity of the sample and  $D$  = apparent translational diffusion coefficient.

### Synthesis of poly(*N*-acryloylmorpholine)<sub>50</sub> (**P1**)

A microwave vial (20 mL) was charged with a magnetic stirrer and 2-(butyl)-thiocarbonylthiopropionic acid (2.83 mL of a 0.5 M solution in 1,4-dioxane, 1.42 mmol), NAM (10 g, 70.80 mmol), VA-044 solution (229  $\mu$ L of a 20 mg mL<sup>−1</sup> in Milli-Q water,  $1.42 \times 10^{-2}$  mmol), and 1,3,5-trioxane (20 mg) as an internal standard were added. The mixture was dissolved in deionized H<sub>2</sub>O (18 mL), the vial was sealed with a rubber septum and deoxygenated by a stream of bubbled nitrogen for 15 min. The vial was then suspended in a preheated oil bath at 50 °C and allowed to stir until no monomer could be detected by <sup>1</sup>H-NMR (DMSO-*d*<sub>6</sub>). Upon completion, the solution was cooled to room temperature and opened to air. The concentration of the solution was determined gravimetrically to be  $6.32 \times 10^{-2}$  mmol g<sup>−1</sup>. <sup>1</sup>H-NMR was performed after lyophilization in CDCl<sub>3</sub>.

<sup>1</sup>H-NMR (CDCl<sub>3</sub>, 300 MHz):  $\delta$  = 3.90–3.05 (m, morpholine), 2.93–2.18 (m, backbone), 2.05–1.02 (m, backbone), and 0.92 (t, <sup>3</sup>J 7.3, CH<sub>3</sub>).

SEC (eluent: DMAc + 0.21% LiCl, PS-standard):  $M_n$ : 6500 g mol<sup>−1</sup>,  $M_w$ : 7100 g mol<sup>−1</sup>, and  $D = 1.09$ .

### Synthesis of poly(*N*-acryloylmorpholine)<sub>100</sub> (**P2**)

**P2** was synthesized according to the procedure described for **P1** with the following amounts:

2-(Butyl)-thiocarbonylthiopropionic acid (1.42 mL of a 0.5 M solution in 1,4-dioxane, 0.708 mmol), NAM (10 g, 70.80 mmol), VA-044 solution (229  $\mu$ L of a 20 mg mL<sup>−1</sup> in Milli-Q water,  $1.42 \times 10^{-2}$  mmol), 1,3,5-trioxane (20 mg), 1,4-dioxane (2.72), and deionized water (10.89).

<sup>1</sup>H-NMR (CDCl<sub>3</sub>, 300 MHz):  $\delta$  = 3.95–3.05 (m, morpholine), 2.90–2.20 (m, backbone), 2.05–1.03 (m, backbone), and 0.90 (t, <sup>3</sup>J 7.2, CH<sub>3</sub>).

SEC (eluent: DMAc + 0.21% LiCl, PS-standard):  $M_n$ : 12 700 g mol<sup>−1</sup>,  $M_w$ : 13 700 g mol<sup>−1</sup>, and  $D = 1.08$ .

### Synthesis of poly[(*N*-acryloylmorpholine)<sub>50</sub>-*b*-(*N*-acryloylthiomorpholine)<sub>30</sub>] micelles (P3)

A microwave vial (20 mL) was charged with a magnetic stirrer and macro-CTA PNAM<sub>50</sub> (1.68 g of a  $6.32 \times 10^{-2}$  mmol g<sup>-1</sup> solution in H<sub>2</sub>O, 0.106 mmol), NAT (0.5 g, 3.18 mmol), VA-044 solution (171  $\mu$ L of a 20 mg mL<sup>-1</sup> in Milli-Q water,  $1.06 \times 10^{-2}$  mmol), and 1,3,5-trioxane (20 mg) as an internal standard were added. The mixture was dissolved in 1,4-dioxane (2.87 mL) and deionized H<sub>2</sub>O (10.55 mL), the vial was sealed with a rubber septum and deoxygenated by a stream of bubbled nitrogen for 15 min. The vial was then suspended in a preheated oil bath at 50 °C and allowed to stir until no monomer could be detected by <sup>1</sup>H-NMR (DMSO-*d*<sub>6</sub>). Upon completion the solution was cooled to room temperature and opened to air. Subsequently, the micelle dispersion was purified by dialysis (MWCO: 3.5–5 kDa) against deionized water for three days including four water exchanges. The concentration of the dispersion was determined gravimetrically (*n* = 3) after lyophilization. <sup>1</sup>H-NMR and SEC analyses were performed after lyophilization.

<sup>1</sup>H-NMR (CDCl<sub>3</sub>, 300 MHz):  $\delta$  = 4.25–3.14 (m, morpholine), 2.98–2.19 (m, backbone), 2.02–1.01 (m, backbone), and 0.95 (t, <sup>3</sup>J 9.3, CH<sub>3</sub>).

SEC (eluent: DMAc + 0.21% LiCl, PS-standard): *M*<sub>n</sub>: 10 900 g mol<sup>-1</sup>, *M*<sub>w</sub>: 11 800 g mol<sup>-1</sup>, and *D* = 1.08.

### Synthesis of poly[(*N*-acryloylmorpholine)<sub>50</sub>-*b*-(*N*-acryloylthiomorpholine)<sub>50</sub>] micelles (P4)

P4 was synthesized according to the procedure described for P3 with the following amounts: macro-CTA PNAM<sub>50</sub> (1.01 g of a  $6.32 \times 10^{-2}$  mmol g<sup>-1</sup> solution in H<sub>2</sub>O, 0.064 mmol), NAT (0.5 g, 3.18 mmol), VA-044 solution (106  $\mu$ L of a 20 mg mL<sup>-1</sup> in Milli-Q water,  $1.06 \times 10^{-2}$  mmol), 1,3,5-trioxane (20 mg), 1,4-dioxane (2.87), and deionized water (10.55).

<sup>1</sup>H-NMR (CDCl<sub>3</sub>, 300 MHz):  $\delta$  = 4.25–3.14 (m, morpholine), 2.98–2.19 (m, backbone), 2.02–1.01 (m, backbone), and 0.95 (t, <sup>3</sup>J 9.3, CH<sub>3</sub>).

SEC (eluent: DMAc + 0.21% LiCl, PS-standard): *M*<sub>n</sub>: 12 500 g mol<sup>-1</sup>, *M*<sub>w</sub>: 14 000 g mol<sup>-1</sup>, and *D* = 1.11.

### Synthesis of poly[(*N*-acryloylmorpholine)<sub>100</sub>-*b*-(*N*-acryloylthiomorpholine)<sub>60</sub>] micelles (P5)

P5 was synthesized according to the procedure described for P3 with the following amounts:

macro-CTA PNAM<sub>100</sub> (1.72 g of a  $3.09 \times 10^{-2}$  mmol g<sup>-1</sup> solution in H<sub>2</sub>O, 0.053 mmol), NAT (0.5 g, 3.18 mmol), VA-044 solution (88.3  $\mu$ L of a 20 mg mL<sup>-1</sup> in Milli-Q water,  $1.06 \times 10^{-2}$  mmol), 1,3,5-trioxane (20 mg), 1,4-dioxane (3 mL), and deionized water (10 mL), 5 h.

<sup>1</sup>H-NMR (CDCl<sub>3</sub>, 300 MHz):  $\delta$  = 4.25–3.14 (m, morpholine), 3.01–2.40 (m, backbone), 2.35–2.10 (m, morpholine), 2.02–1.01 (m, backbone), and 0.95 (t, <sup>3</sup>J 9.3, CH<sub>3</sub>).

SEC (eluent: DMAc + 0.21% LiCl, PS-standard): *M*<sub>n</sub>: 19 400 g mol<sup>-1</sup>, *M*<sub>w</sub>: 21 600 g mol<sup>-1</sup>, and *D* = 1.11.

### Synthesis of poly[(*N*-acryloylmorpholine)<sub>100</sub>-*b*-(*N*-acryloylthiomorpholine)<sub>100</sub>] micelles (P6)

P6 was synthesized according to the procedure described for P3 with the following amounts:

macro-CTA PNAM<sub>100</sub> (1.03 g of a  $3.09 \times 10^{-2}$  mmol g<sup>-1</sup> solution in H<sub>2</sub>O, 0.032 mmol), NAT (0.5 g, 3.18 mmol), VA-044 solution (53  $\mu$ L of a 20 mg mL<sup>-1</sup> in Milli-Q water,  $1.06 \times 10^{-2}$  mmol), 1,3,5-trioxane (20 mg), 1,4-dioxane (5.28 mL), and deionized water (10.56 mL), 8 h.

<sup>1</sup>H-NMR (CDCl<sub>3</sub>, 300 MHz):  $\delta$  = 4.25–3.14 (m, morpholine), 2.99–2.39 (m, backbone), 2.35–2.08 (m, thiomorpholine), 2.02–1.01 (m, backbone), and 0.95 (t, <sup>3</sup>J 9.3, CH<sub>3</sub>).

SEC (eluent: DMAc + 0.21% LiCl, PS-standard): *M*<sub>n</sub>: 23 700 g mol<sup>-1</sup>, *M*<sub>w</sub>: 28 000 g mol<sup>-1</sup>, and *D* = 1.18.

### Kinetic studies

For kinetic investigations, a microwave vial (20 mL) was charged with a magnetic stirrer and the macro-CTA PNAM<sub>100</sub> (2.20 mL of a 0.019 M solution in H<sub>2</sub>O/1,4-dioxane,  $4.24 \times 10^{-2}$  mmol), NAT (0.4 g, 2.54 mmol), VA-044 solution (70.7  $\mu$ L of a 20 mg mL<sup>-1</sup> in Milli-Q water,  $4.24 \times 10^{-3}$  mmol), and 1,3,5-trioxane (20 mg) as an internal standard were added. The mixture was dissolved in 1,4-dioxane (2.87 mL) and deionized H<sub>2</sub>O (10.55 mL), the vial was sealed with a rubber septum and deoxygenated by a stream of bubbled nitrogen for 20 min. The vial was then suspended in a preheated oil bath at 50 °C and allowed to stir for 3.75 h. Every 15 min (30 min for the last two values) a sample was taken, cooled down and analyzed by <sup>1</sup>H-NMR (D<sub>2</sub>O, 300 MHz), SEC (eluent: DMAc + 0.21% LiCl, PS-standard), and DLS (*n* = 3, attenuator: 8, in a pure reaction medium). Monomer conversion was determined by comparing the integrals of the residual vinyl proton signals to the 1,3,5-trioxane standard after the correction of the baseline.

### Oxidative triggered micelle degradation

Polymer dispersions of polymers P3 to P6 were prepared by diluting the polymer stock solution with PBS (10 mM in Milli-Q) to obtain samples with a final volume of 500  $\mu$ L (2 mg mL<sup>-1</sup>). The samples were filtered through a 0.2  $\mu$ m PA syringe filter prior to measurements. Directly before measurements, 500  $\mu$ L of H<sub>2</sub>O<sub>2</sub> solutions with different concentrations (2, 0.2, and 0.02 M) was added and the particle degradation process was monitored by either measuring the mean count rate or the hydrodynamic ratio by DLS. The temperature was set to 37 °C in order to mimic *in vivo* conditions and measurements were performed every 10 min (0.1, 0.01 M H<sub>2</sub>O<sub>2</sub>) and every 5 min (1 M H<sub>2</sub>O<sub>2</sub>). The relative count rate was calculated as the mean count rate divided by the maximum value.

### CMC-determination

The critical micelle concentration (CMC) was determined according to a literature procedure.<sup>47</sup> The fluorescence of Nile red of 10 polymer stock solutions with different concentrations was measured. Therefore, the polymer stock solutions were diluted with Milli-Q water to obtain samples with concen-

trations from  $5 \times 10^{-4}$  to  $0.1 \text{ mg mL}^{-1}$  and a final volume of  $500 \mu\text{L}$ . Then,  $5 \mu\text{L}$  of a Nile red stock solution ( $1 \text{ mg mL}^{-1}$  in THF) was added and the samples were incubated overnight in a thermoshaker device (200 rpm,  $20^\circ\text{C}$ ). After incubation, the fluorescence of Nile red was recorded with a Tecan Reader using a 96 glass well plate at an excitation wavelength of  $535 \pm 10 \text{ nm}$  and an emission wavelength of  $612 \pm 20 \text{ nm}$ . The CMC was determined as the point of intersection of the linear plots in the emission intensity *versus*  $\log c$  spectrum.

### Oxidation-induced micelle degradation and quenching of Nile red

Micelle dispersions of polymers **P3–6** ( $2 \text{ mg mL}^{-1}$ ) were prepared by diluting micelle stock solutions with Milli-Q to obtain samples with a final volume of  $500 \mu\text{L}$ .  $5 \mu\text{L}$  of a Nile red solution in THF ( $1 \text{ mg mL}^{-1}$ ) was added and the samples were incubated overnight in a thermoshaker device (200 rpm,  $20^\circ\text{C}$ ). Prior to measurements, the samples were filtered through a  $0.2 \mu\text{m}$  polyamide (PA) syringe filter to remove possible Nile red aggregates.  $100 \mu\text{L}$  of each sample was diluted with  $100 \mu\text{L}$  of  $\text{H}_2\text{O}_2$  solutions with different concentrations (2, 0.2, and  $0.02 \text{ M}$ ) in a 96 glass well plate. Directly after dilution, the fluorescence of Nile red was recorded with a Tecan Reader using a 96 glass well plate at an excitation wavelength of  $535 \pm 10 \text{ nm}$  and an emission wavelength of  $612 \pm 20 \text{ nm}$ . The temperature was set to  $37^\circ\text{C}$  in order to mimic *in vivo* conditions and measurements were performed every 5 min. The relative fluorescence intensity was calculated as the mean fluorescence intensity divided by the maximum value.

### Cryo-TEM investigations

The measurements were performed on an FEI Tecnai G<sup>2</sup> 20 platform with a LaB6 filament at 200 kV acceleration voltage. Samples were prepared on Quantifoil grids (R2/2) which were treated with Ar plasma prior to use for hydrophilization and cleaning.  $8.5 \mu\text{L}$  of the solutions ( $3 \text{ mg mL}^{-1}$ ) was applied onto the grids utilizing an FEI Vitrobot Mark IV system (offset:  $-5 \text{ mm}$ , blotting time: 1 s). After blotting, the samples were immediately plunged into liquid ethane to obtain vitrification. Samples were transferred to a Gatan cryo stage and subsequently into a Gatan cryo holder (Gatan 626) and were transferred into the microscope by always maintaining a temperature below  $-168^\circ\text{C}$  during the whole transfer and measurement process after vitrification. Images were acquired with a Mega View (OSIS, Olympus Soft Imaging Systems) or an Eagle 4k CCD camera.

### Determination of cytotoxicity

Cytotoxicity studies were performed with the mouse fibroblast cell line L929 (CCL-1, ATCC), as recommended by ISO10993-5. The cells were routinely cultured in Dulbecco's modified eagle's medium with  $2 \text{ mM}$  L-glutamine (Biochrom, Germany) supplemented with 10% fetal calf serum (FCS, Capricorn Scientific, Germany),  $100 \text{ U mL}^{-1}$  penicillin, and  $100 \mu\text{g mL}^{-1}$  streptomycin (Biochrom, Germany) at  $37^\circ\text{C}$  under a humidified 5% (v/v)  $\text{CO}_2$  atmosphere. In detail, cells were seeded at

$1 \times 10^4$  cells per well in a 96-well plate and incubated for 24 h. No cells were seeded in the outer wells. Afterwards, the polymeric suspensions in water were added to the cells at the indicated concentrations (from 1 to  $500 \mu\text{g mL}^{-1}$ ), and the plates were incubated for an additional 24 h. Subsequently, the medium was replaced by a mixture of a fresh culture medium and the resazurin-based solution alamarBlue (Thermo Fisher, Germany, prepared according to the manufacturer's instructions). After further incubation for 4 h at  $37^\circ\text{C}$  under a humidified 5% (v/v)  $\text{CO}_2$  atmosphere, the fluorescence was measured at  $\lambda_{\text{ex}} = 570 \text{ nm}/\lambda_{\text{em}} = 610 \text{ nm}$ , with untreated cells on the same well plate serving as negative controls. The negative control was standardized as 0% of metabolism inhibition and referred to as 100% viability. Cell viability below 70% was considered to be indicative of cytotoxicity. Experiments were conducted in six technical replicates. Data are expressed as the mean  $\pm$  standard deviation (SD) of three independent determinations.

### Uptake studies

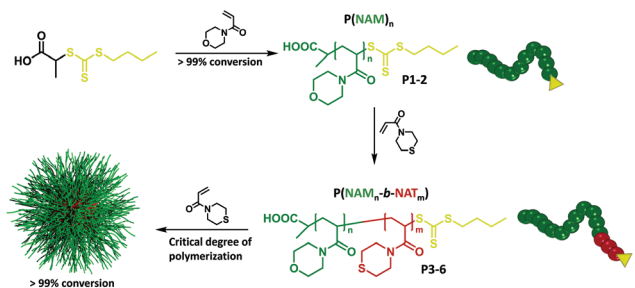
Human embryonic kidney (HEK)-293-T cells (CRL-3216, ATCC) were cultured in Dulbecco's modified eagle's medium with  $2 \text{ mM}$  L-glutamine (Biochrom, Germany) supplemented with 10% FCS (Capricorn Scientific, Germany),  $100 \text{ U mL}^{-1}$  penicillin, and  $100 \mu\text{g mL}^{-1}$  streptomycin (Biochrom, Germany) at  $37^\circ\text{C}$  under a humidified 5% (v/v)  $\text{CO}_2$  atmosphere. For uptake studies, cells were seeded at  $10^5$  cells per mL in 24-well plates and cultured for 24 h. The cells were incubated separately with different concentrations (5, 50 and  $200 \mu\text{g mL}^{-1}$ , respectively) of the micelles at 37 and  $4^\circ\text{C}$  under a humidified 5%  $\text{CO}_2$  atmosphere. The control cells were incubated with a fresh culture medium. The cells were harvested by trypsin treatment in phosphate buffered saline (PBS) supplemented with 1% FCS after 5 min, 4 h and 24 h, respectively. To quench the outer fluorescence of the cells 10% (v/v) trypan blue was added. To determine the relative uptake of the micelles, 10 000 cells were measured by using a Cytomics FC 500 (Beckman Coulter) flow cytometer using gates of forward and side scatterers to exclude the debris and cell aggregates. The sides of viable cells showing the Nile red signal were gated. Data are expressed as the mean  $\pm$  SD of three independent determinations.

## Results and discussion

### Preparation of P(NAM-*b*-NAT) micelles *via* PISA

The PISA technique allows the straightforward preparation of well-defined nanostructures based on amphiphilic block copolymers. In our work, the respective amphiphilic block copolymers were prepared by sequential RAFT chain extension. Hence, NAM served as the hydrophilic block and the hydrophobic block was based on NAT. NAT represents an ideal candidate for the preparation of oxidation-responsive micelles *via* PISA, since the monomer is soluble in water at slightly elevated temperatures ( $>50^\circ\text{C}$ ), but the polymer is insoluble in water





**Scheme 1** Schematic representation of the polymerization and the PISA process to create PNAM-*b*-NAT micelles by sequential RAFT polymerization without any intermediate purification steps.

after polymerization. The micellar shell was based on PNAM, which is known to exhibit excellent biocompatibility and no toxicity.<sup>43,44</sup> NAM can further be polymerized to full conversion in aqueous solutions by RAFT polymerization to obtain well-defined homopolymers with high chain end fidelity, which represents it as an ideal candidate for the preparation of multiblocks in a one-pot approach. Therefore, the first step was prepared in accordance with conditions described in the literature (Scheme 1).<sup>41</sup>

In order to monitor the conversion of the polymerization by <sup>1</sup>H-NMR, 1,3,5-trioxane was added as an internal standard. The high [CTA]/*I*<sub>0</sub> values of 50 and 100 reduce the concentration of active radical species during the RAFT polymerization and therefore guarantee a high degree of active chain ends (>98%, assuming an initiator efficiency of 0.5) after the first polymerization step. Therefore, two NAM homopolymers PNAM<sub>50</sub> (**P1**) and PNAM<sub>100</sub> (**P2**) with [M]<sub>0</sub>/CTA values of 50 and 100, respectively, were synthesized and characterized by <sup>1</sup>H-NMR and SEC (Table 1). The complete disappearance of the monomer signals compared to the internal standard in the <sup>1</sup>H-NMR showed the quantitative conversion of NAM after 4 h. The SEC traces showed monomodal distributions with low dispersities, indicating an excellent control of the polymerization. Because quantitative conversion of NAM was reached, no purification step had to be carried out and the polymer solution could instantly be used for PISA.

For the PISA process, NAT and the initiator were added to the polymer solutions of **P1** and **P2** and the concentration was adjusted by the addition of a 1,4-dioxane/water mixture (20–40% 1,4-dioxane). The presence of 1,4-dioxane was found

to reduce the presence of side-reactions, and polymerizations without 1,4-dioxane resulted in the broadening of the polymer distribution most probably related to the limited flexibility and availability of the growing chain end in the micelle (Fig. S2†). The relatively low [CTA]/*I*<sub>0</sub> value of 10 guaranteed a rapid polymerization progress, while maintaining good control over the polymerization. The conversion of the block copolymerization was monitored *via* <sup>1</sup>H-NMR by comparison of the NAT signals to the internal standard (1,3,5-trioxane). Based on this procedure, micelles with block copolymers of different lengths and block ratios could be obtained (Table 1). All polymerizations showed quantitative conversion within 8 h, as indicated by <sup>1</sup>H-NMR. The successful chain extension was proven by the shift in the SEC curves to lower elution volumes (Fig. 1). The SEC curves of the obtained block copolymers showed monomodal size distribution with low dispersities (*D* < 1.20), demonstrating the good control over the whole process.

After the removal of the 1,4-dioxane and 1,3,5-trioxane by dialysis against deionized water, the micelle dispersions were characterized by DLS and cryo-TEM (Fig. 2) to get information about the diameter and the shape of the nanostructures. Comparison of the size distribution before and after the dialysis step showed only slight differences (Fig. S3†). The change of the diameter of the nanostructures correlates well with the increasing polymer length from P(NAM<sub>50</sub>-*b*-NAT<sub>30</sub>) to P(NAM<sub>100</sub>-*b*-NAT<sub>60</sub>). Interestingly, the size of the micelles increases in a similar way to changing the block ratio (P(NAM<sub>50</sub>-*b*-NAT<sub>30</sub>) *vs.* P(NAM<sub>50</sub>-*b*-NAT<sub>50</sub>)), but also results in a slightly increased dispersity of the sample (Table 2). In order to investigate any potential change of the morphology with varying compositions, cryo-TEM images of both P(NAM<sub>50</sub>-*b*-NAT<sub>30</sub>) and P(NAM<sub>50</sub>-*b*-NAT<sub>50</sub>) were analyzed, which should reveal the structure of the micelle core due to an increased contrast by the sulfur atoms (Fig. 2B and S5†). In both cases, spherical shaped structures were observed. However, an increase of the core size with increasing block lengths of the NAT could be confirmed, which is a result of the longer hydrophobic chain lengths.

In order to analyze the influence of the different block ratios on the stability upon dilution, the CMC was determined by applying Nile red as a fluorescent probe according to a previously published procedure.<sup>47</sup> Therefore, micelle dispersions with different concentrations down to 5 × 10<sup>−4</sup> mg mL<sup>−1</sup> were prepared, incubated with Nile red and the fluorescence intensity was analyzed by fluorescence spectroscopy. The inter-

**Table 1** Summary of the polymers used in this study

Abbrev.	[M] <sub>0</sub> /CTA	[CTA]/ <i>I</i> <sub>0</sub>	Conv. <sup>a</sup> (%)	<i>M</i> <sub>n,th</sub> <sup>b</sup> (g mol <sup>−1</sup> )	<i>M</i> <sub>n,SEC</sub> <sup>c</sup> (g mol <sup>−1</sup> )	<i>D</i> <sup>c</sup>
PNAM <sub>50</sub> ( <b>P1</b> )	50	100	99	7300	6,500	1.09
PNAM <sub>100</sub> ( <b>P2</b> )	100	50	99	12 700	13 700	1.08
P(NAM <sub>50</sub> - <i>b</i> -NAT <sub>30</sub> ) ( <b>P3</b> )	30	10	99	12 000	10 900	1.08
P(NAM <sub>50</sub> - <i>b</i> -NAT <sub>50</sub> ) ( <b>P4</b> )	50	10	99	15 200	12 500	1.11
P(NAM <sub>100</sub> - <i>b</i> -NAT <sub>60</sub> ) ( <b>P5</b> )	60	10	99	23 800	19 400	1.11
P(NAM <sub>100</sub> - <i>b</i> -NAT <sub>100</sub> ) ( <b>P6</b> )	100	10	99	30 100	23 700	1.18

<sup>a</sup> Determined from the ratio of remaining vinyl protons of the monomer to the signals of the internal standard 1,3,5-trioxane. <sup>b</sup> Calculated from the conversion. <sup>c</sup> SEC: DMAc + 0.21 wt% LiCl, PS-calibration.

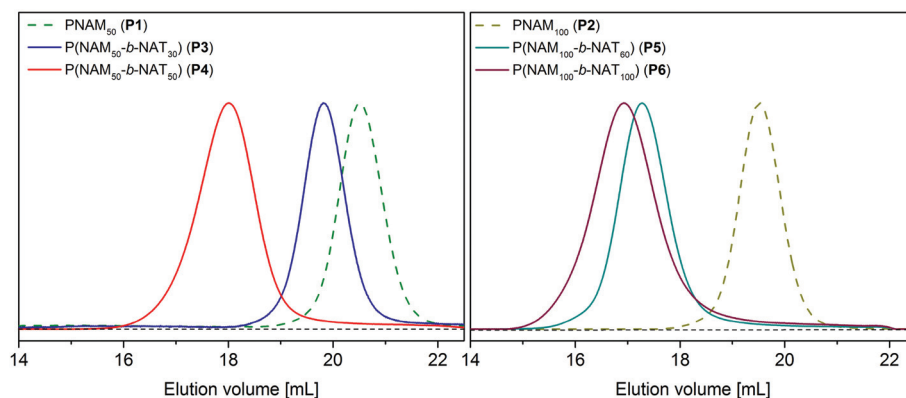


Fig. 1 SEC-curves of homopolymers **P1** to **P2** and block copolymers **P3** to **P6** (DMAc + 0.21 wt% LiCl, PS-standard).

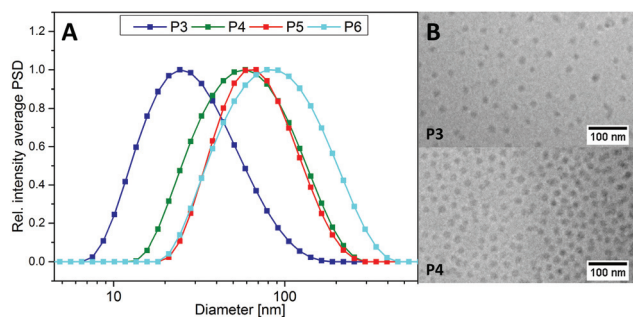


Fig. 2 Characterization of micelles **P3** to **P6** by DLS and cryo-TEM. (A) Intensity average particle size distributions (PSD) determined by DLS;  $n = 3$ ,  $c = 1 \text{ mg mL}^{-1}$  in Milli-Q. (B) cryo-TEM image sections of  $\text{P(NAM}_{50}\text{-}b\text{-NAT}_{30})$  (**P3**) and  $\text{P(NAM}_{50}\text{-}b\text{-NAT}_{50})$  (**P4**). Full pictures can be seen in the ESI (Fig. S7†).

Table 2 Characteristics of micelles based on block copolymers with different block ratios determined by DLS and fluorescence spectroscopy

Abbrev.	wt% NAM	wt% NAT	$R_h^a$ ( $d$ , nm)	$R^b$ ( $d$ , nm)	PDI <sup>a</sup>	CMC <sup>c</sup> ( $\mu\text{g mL}^{-1}$ )
<b>P3</b>	60	40	25.04	16.11	0.225	15
<b>P4</b>	47	53	50.41	16.91	0.235	16
<b>P5</b>	60	40	61.34	17.55	0.207	17
<b>P6</b>	47	53	72.88	25.76	0.242	16

<sup>a</sup> Determined by DLS ( $n = 3$ ,  $c = 1 \text{ mg mL}^{-1}$ ). <sup>b</sup> Determined by cryo-TEM analysis (measurement of >100 samples, Fig. S7). <sup>c</sup> Determined by fluorescence spectroscopy (Fig. S4).

section of the linear fits of the plot of the intensity as a function of the logarithm of the polymer concentration was described as the CMC of the sample (Fig. S4† and Table 2). All polymers revealed CMCs in the range of  $15\text{--}17 \mu\text{g mL}^{-1}$ . Therefore, the increase of the hydrophobic content from polymer **P3** to **P6** did not seem to significantly affect the CMC of the micelles.

Kinetic investigations on the PISA were performed with the aim to gain a deeper insight into the mechanism of the micelle formation during the polymerization. Therefore,

samples were taken at regular time intervals from the polymerization mixture and analyzed for monomer conversion ( $^1\text{H-NMR}$ ), molar mass distribution (SEC) and micelle formation (DLS). Interestingly, the time-dependent kinetics of the conversion shows a nearly sigmoidal plot (Fig. 3A), which is typical of emulsion polymerization and not the linear increase, which is expected for the quasi-linear region of RAFT polymerization.<sup>48,49</sup> After an initial retardation time, the rate of polymerization increases first slowly, but then continuously, which is most probably related to an increased number of polymer particles or micelles, respectively. The polymerization then occurs mostly within these micelles, and, similar to an emulsion polymerization termination reaction might be decreased. Nevertheless, the  $M_n$  increases linearly with the conversion and low dispersities are maintained, which proves the living character of the RAFT polymerization (Fig. 3B). Moreover, the shift of the mono-modal elution curves did not show the presence of any prominent side-reactions (Fig. 3C). Parallel to the increase of molar mass, micelle formation was observed by the increase of the count rate (Fig. 3D).

### Cytotoxicity and uptake studies

In order to investigate the biocompatibility of the novel carrier, the cytotoxicity of the micelles **P3** to **P6** was investigated by AlamarBlue assays. In addition, the uptake of the exemplarily chosen micelles **P3** was examined by fluorescence correlation spectroscopy using HEK cells. All polymers **P3** to **P6** showed no toxic effect on L929 cells up to a concentration of  $500 \mu\text{g mL}^{-1}$  (Fig. S5A†), while the fluorescence studies confirm the uptake into cells (Fig. S5B†). These results confirm the reported high biocompatibility and non-toxicity of PNAM and further prove the suitability of PNAT for the preparation of oxidation-responsive carrier systems (Scheme 2). Moreover, we analyzed the toxicity of the oxidized form of polymer **P3**. Again, no toxicity was observed up to  $500 \mu\text{g mL}^{-1}$ .

### Oxidation-induced degradation

The ability of thioethers in polymers to undergo oxidation by ROS is in most cases simulated by the addition of hydrogen

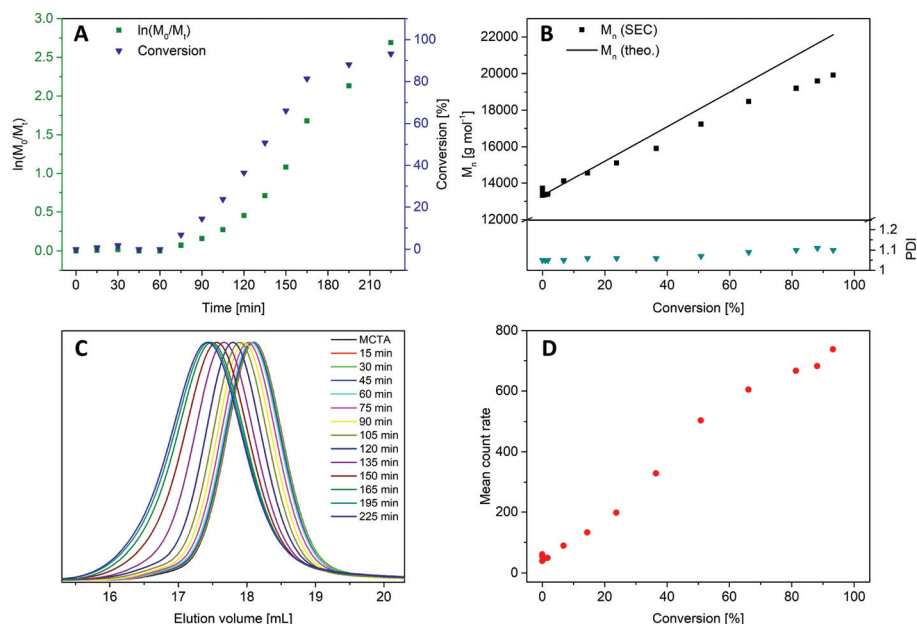
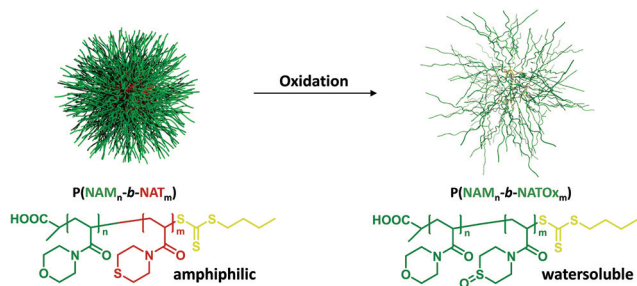


**Fig. 3** Kinetic studies of the PISA of P(NAM-b-NAT) (A) Plot of the time-dependent increase of  $\ln(M_0/M_t)$  and monomer conversion, which was determined by  $^1\text{H}$ -NMR using 1,3,5-trioxane as an internal standard. (B) Molar mass and dispersity, which was determined by SEC (eluent: DMAc + 0.21 wt% LiCl, PS-standard) and the theoretical molar mass (calculated by  $[(M_0/[M_0]^{-1}) \times M_{\text{NAT}}] + M_{\text{MCTA}}$ ) in dependence on the monomer conversion. (C) SEC curves of the polymerization mixture after different polymerization times. (D) The increase of the mean count rate, determined by DLS measurements ( $n = 3$ ) of the polymerization mixture, in dependence on the monomer conversion.



**Scheme 2** Schematic representation of the oxidation-induced degradation process by oxidation of NAT to NATOx.

peroxides or hypochlorites as these are typical and easy available species found in inflammatory reactions.<sup>50</sup> As previously mentioned, the concentration of these oxidative compounds can be in the millimolar range in inflamed tissue. In order to check the responsiveness of our system to biologically relevant conditions, micelle dispersions of **P3** to **P6** were prepared and mixed with  $\text{H}_2\text{O}_2$  solutions to establish concentrations of 1, 0.1 and 0.01  $\text{mol L}^{-1}$ .

The degradation process was monitored by DLS measurements, since the amount of micelles could be directly correlated with the mean count rate (Fig. 4) and the simultaneous cumulant analysis gave information on the development of the micelle diameter (Fig. S6†). Measurements were performed at 37 °C in PBS in order to mimic the conditions in a biological environment.

In all cases, a degradation of the micelles could be detected upon exposure to  $\text{H}_2\text{O}_2$ . The decrease of the mean count rate followed a sigmoidal trend. After exposure, a certain delay time was detected, in which the count rate remained nearly constant. At a certain point, the decrease of the count rate started to take place. We observed that the count rate decreased in an accelerating manner. The detected degradation profiles matched to the trend of an auto-accelerating process. Since hydrogen peroxide is a strongly hydrophilic oxidant, the oxidation reaction is mainly determined by the diffusion of  $\text{H}_2\text{O}_2$  molecules in the hydrophobic NAT micelle core, which certainly increases with the ratio of the oxidized monomer units due to the increasing hydrophilicity. However, when the oxidation of NAT inside the micelles reach a critical value, the core becomes hydrophilic and finally completely soluble in the aqueous environment. The parallel decrease of both the count rate and the diameter suggests that the micelles did not degrade in an erosive process, but burst rather abruptly when a certain degree of oxidation was reached.

Since the micelle degradation curves showed the typical profile of an auto-accelerating reaction, the decay in the count rate could be described with a Boltzmann function.<sup>51,52</sup> Based on the Boltzmann fit, the half-life times of the degradation processes of the micelles **P3** to **P6** for the different  $\text{H}_2\text{O}_2$  concentrations could be determined (Fig. 4D). For the micelles with shorter hydrophobic blocks, the degradation was more rapid as indicated by smaller half-life times. Smaller NAT blocks also led to a reduction of the delay time and hence a more instant degradation profile. These effects are most prob-

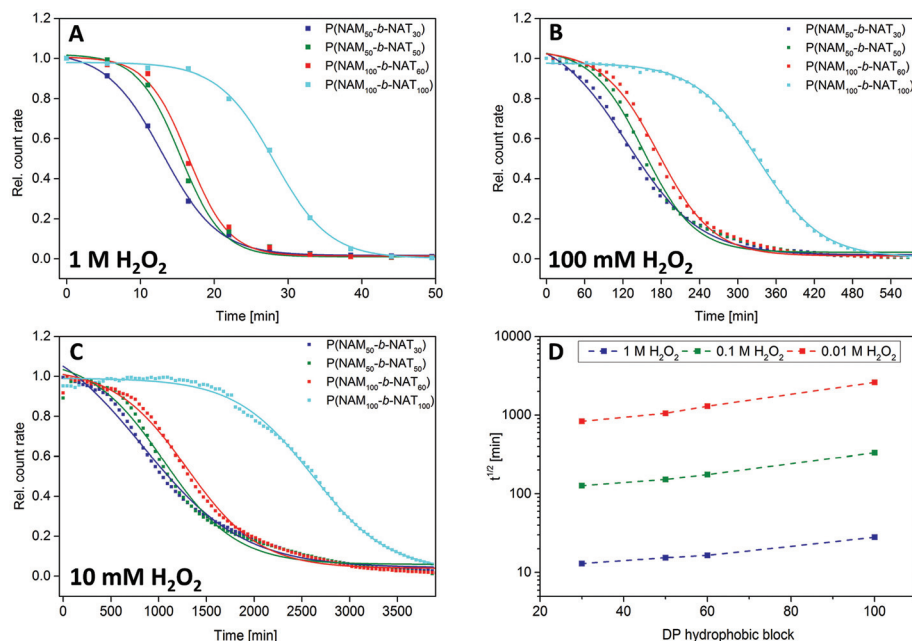


**Fig. 4** Oxidation-induced degradation of micelles P3 to P6 analyzed by DLS (37 °C, in PBS). (A) The time-dependent decrease of the count rate at 1 M  $\text{H}_2\text{O}_2$ . (B) The time-dependent decrease of the count rate at 100 mM  $\text{H}_2\text{O}_2$ . (C) The time-dependent decrease of the count rate at 10 mM  $\text{H}_2\text{O}_2$ . (D) Comparison of the half-life times determined by a Boltzmann fit for different degrees of polymerization (DP) of the hydrophobic block.

ably related to the higher surface/volume ratio of micelles, which results in a much faster penetration of  $\text{H}_2\text{O}_2$  molecules.<sup>13</sup> Comparing the logarithm of the half-life times with the degree of polymerization of the hydrophobic blocks revealed a nearly linear trend (Fig. 4D). The half-life times seemed to be mainly dependent on the length of the hydrophobic block, without being much affected by the block ratio. This direct correlation gives a handle to conveniently tune the degradation profile of the carrier system and adjust it to the desired target.

#### Oxidation triggered fluorescence quenching

In addition to the DLS studies, the change in the characteristics of the NAT in the micelle core was analyzed by a fluo-

rescence intensity change of encapsulated Nile red, which is quenched in an aqueous environment. Furthermore, such an assay is often used as a model study to simulate the release of an encapsulated hydrophobic drug.<sup>13,14,16</sup> As in the DLS studies, different concentrations of  $\text{H}_2\text{O}_2$  (1, 0.1, 0.01 M) were used to imitate the presence of oxidative stress. Upon oxidation of the NAT block, the micelle core should become increasingly hydrophilic and therefore result in the quenching of the fluorescence of Nile red. The decrease of the fluorescence intensity over time was monitored by fluorescence spectroscopy. The results demonstrate that the fluorescence intensity of Nile red decreased over time, which correlated well with the concentration of added  $\text{H}_2\text{O}_2$  (Fig. 5 and S7–S10†).

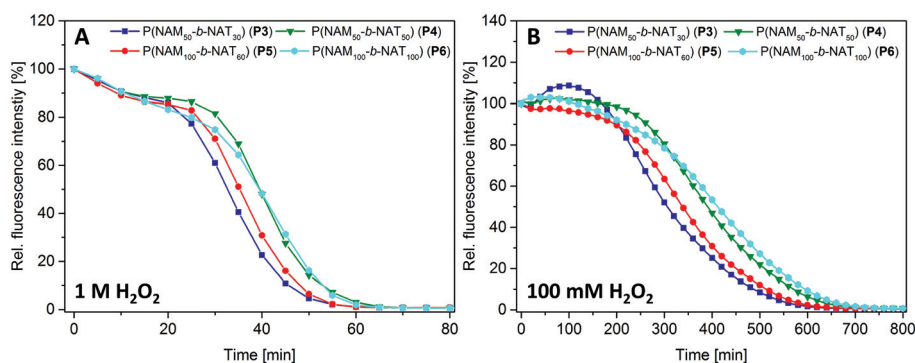


**Fig. 5** Oxidation-induced fluorescence quenching of Nile red encapsulated in micelles P3 to P6, which was analyzed by fluorescence spectroscopy (37 °C). (A) The time-dependent decrease of the fluorescence intensity at 1 M  $\text{H}_2\text{O}_2$ . (B) The time-dependent decrease of the fluorescence intensity at 100 mM  $\text{H}_2\text{O}_2$ .



However, in comparison with the degradation kinetics determined by DLS, the fluorescence quenching is considerably delayed. This effect might either be caused by the reduced diffusion of the hydrogen peroxide into the core due to the present hydrophobic dye or a still persistent coordination of the dye in the remaining hydrophobic segments of the polymer even after reaching the critical degree of oxidation for micellation. All curves showed a small increase in intensity after the start of the measurement, which might be associated with heating effects (room temperature to 37 °C) resulting in an enhanced fluorescence of Nile red. Moreover, it is noteworthy to mention, that the observed quenching rates are not dependent on the DP of the hydrophobic block as observed in the DLS studies, but on the balance of hydrophilic and hydrophobic blocks. Consequently, the polymers **P3** and **P5** with a block mass ratio of 60 : 40% exhibited the fastest fluorescence quenching, whereas **P4** and **P6** with a ratio of 47 : 53% showed a slower intensity decrease. This difference might again be related to the changed kinetics of the degradation in the presence of the hydrophobic dye, but almost similar quenching behavior of all four micelles might also indicate that the dye is only infiltrating the surface of the core, especially in the case of **P6**. The detailed investigation of this effect, however, requires further studies, which are currently ongoing. Nevertheless, all measurements ended up with a relative fluorescence intensity of below 1%, indicating the quantitative degradation of the micelles and a complete change of the thioether moieties.

## Conclusion and outlook

The presented work not only demonstrates that polymerization-induced self-assembly can be combined with highly reactive monomers to create block copolymers using a one-pot approach circumventing tedious purification steps, but also provides convenient access to tunable oxidation-responsive micelles for targeted drug delivery. The monomer NAM enables a fast and efficient preparation of the first hydrophilic block with high chain-end retention in the RAFT process at quantitative conversion and guarantees an excellent biocompatibility for the final micellar structures. The structurally similar and water-soluble monomer NAT features a similar high reactivity in the aqueous polymerization but results in the formation of a hydrophobic block, which makes it an excellent candidate for the PISA process. Due to the near quantitative conversions in both reactions and the PISA process we were able to prepare micelles consisting of the amphiphilic block copolymer P(NAM-*b*-NAT) without any intermediate purification steps. Moreover, we were able to tune the size of the resulting micelles by varying the size of the overall polymer or the composition of the polymer, which mainly affects the size of the micelle core. The characterization by DLS and cryo-TEM revealed spherical shapes in all examined compositions, despite the hydrophobic contents being more than 50 wt%.

In addition, the thioether moiety in PNAT can be oxidized to a very hydrophilic sulfoxide by common ROS species such as hydrogen peroxide yielding in the disassembly of the micelles. Kinetic studies of the oxidation-induced degradation process by DLS measurements revealed complete micelle degradation for all selected systems even at low H<sub>2</sub>O<sub>2</sub> concentrations of 10 mM. The degradation kinetics were described as an auto-accelerating process, which was mainly dependent on the length of the hydrophobic block. Moreover, spectroscopy studies on the fluorescence quenching of Nile red, which was encapsulated in the micelles, further confirm the oxidation of the hydrophobic PNAT in the presence of hydrogen peroxide and the resulting disintegration of the micelles.

As all materials, including the oxidized polymer, reveal no cytotoxicity, we are convinced that the presented system represents an interesting and versatile new platform for the selective delivery of drugs to sites of high oxidative stress. Further research is certainly required to investigate reversible cross-linking methods or possibilities to vary the shape of the nanostructures, but the here reported effective preparation of the final structures within less than 8 hours starting from the monomers will facilitate further developments on this oxidation-responsive carrier material.

## Author contributions

The manuscript was written through contributions from all authors. All authors have given approval to the final version of the manuscript.

## Conflicts of interest

There are no conflicts to declare.

## Acknowledgements

The funding of the collaborative research center PolyTarget (SFB 1278) by the Deutsche Forschungsgemeinschaft (DFG) is highly acknowledged. Johannes C. Brendel further thank the DFG for funding from the Emmy-Noether Programme (BR 4905/3-1) and support by the FCI (Fonds der Chemischen Industrie). Cryo-TEM investigations were performed at the Electron Microscopy facilities of the Jena Center for Soft Matter (JCSM), which was established with grants from the DFG and the European Fund for Regional Development (EFRE).

## References

- 1 M. Valko, D. Leibfritz, J. Moncol, M. T. Cronin, M. Mazur and J. Telser, *Int. J. Biochem. Cell Biol.*, 2007, **39**, 44–84.
- 2 K. Apel and H. Hirt, *Annu. Rev. Plant Biol.*, 2004, **55**, 373–399.

- 3 C. E. MacKay and G. A. Knock, *J. Physiol.*, 2015, **593**, 3815–3828.
- 4 V. J. Thannickal and B. L. Fanburg, *Am. J. Physiol.: Lung Cell. Mol. Physiol.*, 2000, **279**, 1005–1028.
- 5 F. Giacco and M. Brownlee, *Circ. Res.*, 2010, **107**, 1058–1070.
- 6 M. Valko, C. J. Rhodes, J. Moncol, M. Izakovic and M. Mazur, *Chem.-Biol. Interact.*, 2006, **160**, 1–40.
- 7 R. Zhou, A. S. Yazdi, P. Menu and J. Tschopp, *Nature*, 2011, **469**, 221–225.
- 8 I. Bjarnason, J. Hayllar, A. J. MacPherson and A. S. Russell, *Gastroenterology*, 1993, **104**, 1832–1847.
- 9 D. A. Peura and L. Goldkind, *Arthritis Res. Ther.*, 2005, **7**, 7–13.
- 10 H. Schäcke, W.-D. Döcke and K. Asadullah, *Pharmacol. Ther.*, 2002, **96**, 23–43.
- 11 Q. Xu, *et al.*, *Macromol. Biosci.*, 2016, **16**, 635–646.
- 12 M. Valko, H. Morris and M. T. D. Cronin, *Curr. Med. Chem.*, 2005, **12**, 1161–1208.
- 13 R. d'Arcy, A. Siani, E. Lallana and N. Tirelli, *Macromol.*, 2015, **48**, 8108–8120.
- 14 M. K. Gupta, T. A. Meyer, C. E. Nelson and C. L. Duvall, *J. Controlled Release*, 2012, **162**, 591–598.
- 15 M. Tang, P. Hu, Q. Zheng, N. Tirelli, X. Yang, Z. Wang, Y. Wang, Q. Tang and Y. He, *J. Nanobiotechnol.*, 2017, **15**, 39.
- 16 A. Y. Kim, J. H. Ha and S. N. Park, *Biomacromolecules*, 2017, **18**, 3197–3206.
- 17 G. Chen, H. Deng, X. Song, M. Lu, L. Zhao, S. Xia, G. You, J. Zhao, Y. Zhang, A. Dong and H. Zhou, *Biomaterials*, 2017, **144**, 30–41.
- 18 P. Han, N. Ma, H. Ren, H. Xu, Z. Li, Z. Wang and X. Zhang, *Langmuir*, 2010, **26**, 14414–14418.
- 19 N. Ma, Y. Li, H. Ren, H. Xu, Z. Li and X. Zhang, *Polym. Chem.*, 2010, **1**, 1609–1614.
- 20 H. Ren, Y. Wu, N. Ma, H. Xu and X. Zhang, *Soft Matter*, 2012, **8**, 1460–1466.
- 21 C. de Gracia Lux, S. Joshi-Barr, T. Nguyen, E. Mahmoud, E. Schopf, N. Fomina and A. Almutairi, *J. Am. Chem. Soc.*, 2012, **134**, 15758–15764.
- 22 A. T. Franks and K. J. Franz, *Chem. Commun.*, 2014, **50**, 11317–11320.
- 23 D. Zhang, Y. Wei, K. Chen, X. Zhang, X. Xu, Q. Shi, S. Han, X. Chen, H. Gong, X. Li and J. Zhang, *Adv. Healthcare Mater.*, 2015, **4**, 168–168.
- 24 A. Napoli, M. Valentini, N. Tirelli, M. Muller and J. A. Hubbell, *Nat. Mater.*, 2004, **3**, 183–189.
- 25 C. Xiao, J. Ding, L. Ma, C. Yang, X. Zhuang and X. Chen, *Polym. Chem.*, 2015, **6**, 738–747.
- 26 J. Herzberger, K. Fischer, D. Leibig, M. Bros, R. Thiermann and H. Frey, *J. Am. Chem. Soc.*, 2016, **138**, 9212–9223.
- 27 C. Gao, Q. Li, Y. Cui, F. Huo, S. Li, Y. Su and W. Zhang, *J. Polym. Sci., Part A: Polym. Chem.*, 2014, **52**, 2155–2165.
- 28 W.-M. Wan and C.-Y. Pan, *Polym. Chem.*, 2010, **1**, 1475–1484.
- 29 Y. Li and S. P. Armes, *Angew. Chem., Int. Ed.*, 2010, **49**, 4042–4046.
- 30 L. P. D. Ratcliffe, B. E. McKenzie, G. M. D. Le Bouëdec, C. N. Williams, S. L. Brown and S. P. Armes, *Macromol.*, 2015, **48**, 8594–8607.
- 31 Y. Xu, Y. Li, X. Cao, Q. Chen and Z. An, *Polym. Chem.*, 2014, **5**, 6244–6255.
- 32 Z. An, Q. Shi, W. Tang, C.-K. Tsung, C. J. Hawker and G. Stucky, *J. Am. Chem. Soc.*, 2007, **129**, 14493–14499.
- 33 Y. Pei, A. B. Lowe and P. J. Roth, *Macromol. Rapid Commun.*, 2017, **38**, 1600528.
- 34 M. Lansalot, J. Rieger and F. D'Agosto, Polymerization-Induced Self-Assembly: The Contribution of Controlled Radical Polymerization to The Formation of Self-Stabilized Polymer Particles of Various Morphologies, in *Macromolecular Self-assembly*, ed. L. Billon and O. Borisov, John Wiley & Sons, Inc., Hoboken, New Jersey, 2016, pp. 33–82.
- 35 B. Charleux, G. Delaittre, J. Rieger and F. D'Agosto, *Macromol.*, 2012, **45**, 6753–6765.
- 36 B. Karagoz, C. Boyer and T. Davis, *Macromol. Rapid Commun.*, 2014, **35**, 417–421.
- 37 B. Karagoz, L. Esser, H. T. Duong, J. S. Basuki, C. Boyer and T. P. Davis, *Polym. Chem.*, 2014, **5**, 350–355.
- 38 W.-M. Wan, C.-Y. Hong and C.-Y. Pan, *Chem. Commun.*, 2009, **39**, 5883–5885.
- 39 I. Chaduc, E. Reynaud, L. Dumas, L. Albertin, F. D'Agosto and M. Lansalot, *Polym.*, 2016, **106**, 218–228.
- 40 J. Lesage de la Haye, X. Zhang, I. Chaduc, F. Brunel, M. Lansalot and F. D'Agosto, *Angew. Chem., Int. Ed.*, 2016, **55**, 3739–3743.
- 41 G. Gody, T. Maschmeyer, P. B. Zetterlund and S. Perrier, *Nat. Commun.*, 2013, **4**, 2505.
- 42 I. Dalle-Donne, R. Rossi, R. Colombo, D. Giustarini and A. Milzani, *Clin. Chem.*, 2006, **52**, 601–623.
- 43 H. Takahashi, M. Nakayama, K. Itoga, M. Yamato and T. Okano, *Biomacromolecules*, 2011, **12**, 1414–1418.
- 44 W. Li, M. Nakayama, J. Akimoto and T. Okano, *Polymer*, 2011, **52**, 3783–3790.
- 45 P. Hennaux and A. Laschewsky, *Colloid Polym. Sci.*, 2003, **281**, 807–814.
- 46 S. C. Larnaudie, J. C. Brendel, K. A. Jolliffe and S. Perrier, *J. Polym. Sci., Part A: Polym. Chem.*, 2016, **54**, 1003–1011.
- 47 M. K. Gupta, T. A. Meyer, C. E. Nelson and C. L. Duvall, *J. Controlled Release*, 2012, **162**, 591–598.
- 48 A. Matsumoto, K. Kodama, H. Aota and I. Capek, *Eur. Polym. J.*, 1999, **35**, 1509–1517.
- 49 G. Moad, E. Rizzardo and S. H. Thang, *Acc. Chem. Res.*, 2008, **41**, 1133–1142.
- 50 S. Joshi-Barr, C. de Gracia Lux, E. Mahmoud and A. Almutairi, *Antioxid. Redox Signaling*, 2014, **21**, 730–754.
- 51 J. Li, W. Ke, L. Wang, M. Huang, W. Yin, P. Zhang, Q. Chen and Z. Ge, *J. Controlled Release*, 2016, **225**, 64–74.
- 52 V. Khutoryanskiy and N. Tirelli, *Pure Appl. Chem.*, 2007, **80**, 1703–1718.